Extremophiles (2009) 13:461–470
DOI 10.1007/s00792-009-0231-9

ORIGINAL PAPER

Structural determinants of the high thermal stability of *Sso*Pox from the hyperthermophilic archaeon *Sulfolobus solfataricus*

Pompea Del Vecchio · Mikael Elias · Luigia Merone · Giuseppe Graziano · Jérôme Dupuy · Luigi Mandrich · Paola Carullo · Bertrand Fournier · Daniel Rochu · Mosè Rossi · Patrick Masson · Eric Chabriere · Giuseppe Manco

Received: 7 January 2009 / Accepted: 4 February 2009 / Published online: 27 February 2009
© Springer 2009

Abstract Organophosphates (OPs) constitute the largest class of insecticides used worldwide and certain of them are potent nerve agents. Consequently, enzymes degrading OPs are of paramount interest, as they could be used as bioscavengers and biodecontaminants. Looking for a stable OPs catalyst, able to support industrial process constraints, a hyperthermophilic phosphotriesterase (PTE) (*Sso*Pox) was isolated from the archaeon *Sulfolobus solfataricus* and was found to be highly thermostable. The solved 3D structure revealed that *Sso*Pox is a noncovalent dimer, with lactonase activity against "quorum sensing signals", and therefore could represent also a potential weapon against certain pathogens. The structural basis of the high thermostability of *Sso*Pox has been investigated by performing a careful comparison between its structure and that of two mesophilic PTEs from *Pseudomonas diminuta* and *Agrobacterium radiobacter*. In addition, the conformational stability of *Sso*Pox against the denaturing action of temperature and GuHCl has been determined by means of circular dichroism and fluorescence measurements. The data suggest that the two fundamental differences between *Sso*Pox and the mesophilic counterparts are: (a) a larger number of surface salt bridges, also involved in complex networks; (b) a tighter quaternary structure due to an optimization of the interactions at the interface between the two monomers.

Keywords Hyperthermophilic enzyme · Conformational stability · Salt bridges · Quaternary structure organization

Abbreviations

OPs	Organophosphates
PTE	Phosphotriesterase
OPD	Organophosphate-degrading
PLL	Phosphotriesterase-like lactonase

Pompea Del Vecchio, Mikael Elias and Luigia Merone were contributed equally to this paper.

Communicated by T. Matsunaga.

P. Del Vecchio · P. Carullo
Dipartimento di Chimica "Paolo Corradini",
Università di Napoli "Federico II", Via Cintia,
80126 Naples, Italy

M. Elias · E. Chabriere
Architecture et Fonction des Macromolécules Biologiques,
CNRS-Université de la Méditerranée, 13288 Marseille, France

L. Merone · L. Mandrich · M. Rossi · G. Manco (✉)
Istituto di Biochimica delle Proteine,
Consiglio Nazionale delle Ricerche,
Via P. Castellino 111, 80131 Naples, Italy
e-mail: g.manco@ibp.cnr.it

G. Graziano
Dipartimento di Scienze Biologiche ed Ambientali,
Università del Sannio, 82100 Benevento, Italy

J. Dupuy
Laboratoire de Cristallogenèse et Cristallographie des
Protéines, Institut de Biologie Structurale JP EBEL,
38027 Grenoble, France

B. Fournier
Laboratoire de Cristallographie et Modélisation des Matériaux
Minéraux et Biologiques, CNRS-Université Henri Poincaré,
54506 Nancy, France

D. Rochu · P. Masson · E. Chabriere
Unité d'Enzymologie, Département de Toxicologie,
Centre de Recherches du Service de Santé des Armées,
38702 La Tronche, France

Introduction

Organophosphates (OPs) are well known potent toxic compounds because they irreversibly inhibit acetylcholinesterase, a key enzyme of the central nervous system. They have been extensively used since the end of World War II. Their toxic properties have been exploited for the development of chemical warfare agents such as sarin, soman and VX and mostly for the development of agricultural insecticides (Raushel 2002). Enzymes that are capable of degrading these OPs, are therefore attractive as potential anti-dotes because of their intrinsic potential in decontamination/detection systems for organophosphate-based pesticides and nerve agents (Merone et al. 2008; Singh 2009). Enzymatic detoxification of OPs has become the subject of numerous studies because current methods of removing them, such as bleach treatments and incineration, are slow, expensive and cause environmental concerns. For this application, OP hydrolases are appealing due to their broader substrate specificity and higher catalytic rate (LeJeune et al. 1998).

Enzymes that catalyze the hydrolysis of phosphoester bonds in OPs are known from several different organisms. In a strain of *Alteromonas*, an organophosphate-degrading (OPD) enzyme belonging to the prolidase family, named organophosphorus acid anhydrolase, was identified (Cheng et al. 1993). Another enzyme isolated from *Loligo vulgaris* is diisopropylfluorophosphatase, which prefers P–F bonds. Its three-dimensional structure was solved and reveals a six-bladed β-propeller with two calcium ions in a central water-filled tunnel (Koepke et al. 2002). The HDL-associated human paraoxonase hydrolyses phosphotriesters too, albeit with lower proficiency. The structure of a chimeric mammalian recombinant paraoxonase-1 was recently solved, and shows a similar fold as those of diisopropylfluorophosphatase (Harel et al. 2004). Some other microbial enzymes (EC 3.1.8.1) generally called phosphotriesterases (PTEs), or sometimes organophosphorous hydrolases, organo-phosphate-degrading enzymes, parathion hydrolases (Hou et al. 1996) or paraoxonases (Merone et al. 2005), show preference for organophosphorous compounds with P–O or P–S bonds. PTEs are members of the amidohydrolases superfamily (Seibert and Raushel 2005), enzymes catalyzing hydrolysis of a broad range of compounds with different chemical properties (phosphoesters, esters, amides, etc.). Their coding genes, *opd* (*o*rgano *p*hosphate *d*egradation), were isolated in *Pseudomonas diminuta* (Munnecke 1976), *Flavobacterium* sp. (Sethunathan and Yoshida 1973), *Agrobacterium radiobacter* (Horne et al. 2003), and genes similar to *opd* were also identified in Archaea (Merone et al. 2008).

Since the synthesis of their most preferred substrate, paraoxon, was described in 1950s, it has been postulated that PTEs might have evolved specifically to the present high catalytic efficiency over a relative short period of time (Ghanem and Raushel 2005). The catalytic properties of PTEs are extensively studied because of their ability to hydrolyze pesticides and several nerve agents. The first complete catalytic mechanism for PTEs was proposed by Aubert et al. (2004). Although this mechanism has been a cornerstone, it suffered from various limits and different catalytic mechanisms have recently been proposed (Jackson et al. 2005; Jackson et al. 2008; Elias et al. 2008; Wong and Gao 2007).

Extremophiles are appealing in order to obtain an efficient and low cost bioscavenger of organophosphorous compounds. In last decades there has been an increase in the discovery, isolation, and investigation of organisms inhabiting extreme environments (Rothschild and Mancinelli 2001). Among these, organisms living at high temperatures (thermophiles and hyperthermophiles) are of particular interest since proteins from these organisms can function and remain stable at or near extreme temperatures and generally are endowed with resistance to other stressing conditions (Jaenicke and Bohm 1998). These proteins have potential in industry directly or as models for engineering proteins because their unique properties, such as activity at extreme temperatures or in the presence of organic solvents or detergents at moderate temperature, are often desirable for industrial processes (Bruins et al. 2001; Demirjian et al. 2001). They represent also an unique opportunity to study relationships between stability, dynamics and function of proteins (Ladenstein and Antranikian 1998; D'Amico et al. 2003).

Looking for a thermostable enzyme able to hydrolyze OPs, *Sso*Pox has been isolated from the hyperthermophilic archaeon *Sulfolobus solfataricus* and kinetically characterized (Merone et al. 2005). The protein displays 30% sequence identity with mesophilic PTEs. In view of its PTE activity, *Sso*Pox was initially related to the PTE family, but biochemical and phylogenetic evidences suggested that *Sso*Pox belongs to another close protein family, that of phosphotriesterase-like lactonase (PLL) (Afriat et al. 2006). The X-ray structure of *Sso*Pox and kinetic properties revealed that it is a lactonase with promiscuous PTE activity (Elias et al. 2007, 2008). This property has permitted to trace a potential evolution pathway from lactonases, such as *Sso*Pox, to the actual optimized mesophilic PTEs in the last 50 years (Afriat et al. 2006). *Sso*Pox is a highly thermostable enzyme, with denaturation half-lives of 4 h and 90 min at 95 and 100°C, respectively. This property facilitates rapid high yield purification of recombinant enzyme heterologously expressed by heating cell lysates and then precipitating mesophilic host proteins (Merone et al. 2005). Owing to its thermostability and rare properties, *Sso*Pox is considered as an excellent starting point for biotechnological applications directed towards the

achievement of efficient bioscavengers for organophosphorus compounds and against certain pathogens. In fact a number of microbial pathogens use "quorum sensing" to infect the host and "quorum quenching" due to specific lactonases may represent a valid tool (Dong et al. 2001).

In this work a careful comparison between the 3D structure of *Sso*Pox and the two mesophilic PTEs from *P. diminuta* and *A. radiobacter* was performed with the aim to identify the possible structural determinants of the high thermal stability of the hyperthermophilic enzyme. In addition, the conformational stability of *Sso*Pox with respect to temperature and GuHCl has been investigated by means of circular dichroism.

Materials and methods

Structural analysis

The structures of *Sso*Pox in apo form and in complex with a quorum-sensing lactone mimic, pdb codes 2vc5 and 2vc7, respectively, were taken from Elias et al. (2008). The pdb code of *P. diminuta* PTE is 1dpm, those of *A. radiobacter* PTE are 2d2h and 2d2j. Structural analysis and comparison, cartoon and ribbon representations of protein structures were made using PyMOL (DeLano 2002). Hydrogen atoms were automatically generated with REFMAC (Murshudov et al. 1997). The electrostatic potential grid of *Sso*Pox was obtained with MoPro using a multipolar atomic model (Guillot et al. 2001). The charge density parameters were transferred from the multipolar atomic database (Pichon-Pesme et al. 2004). The molecular surface was computed with PyMOL using a solvent probe of 1.4 Å radius and the imported electrostatic potential grid was mapped to it. Surface contact between monomers was computed using the Protein–Protein Interaction Server (V. 1.5) (Jones and Thornton 1996). Computational studies of accessible surface, total surface and volumes were performed using VADAR web server (V. 1.4; Willard et al. 2003). The total number of hydrogen bonds was determined with *HBPLUS* (McDonald and Thornton 1994). Root mean square deviations (r.m.s.d.) were computed using Swiss-pdb-viewer (Guex and Peitsch 1997).

Circular dichroism

CD spectra were recorded with a Jasco J-715 spectropolarimeter equipped with a Peltier type temperature control system (Model PTC-348WI). Molar ellipticity per mean residue, $[\theta]$ in deg cm^2 dmol^{-1}, was calculated from the equation: $[\theta] = [\theta]_{obs}$ mrw/10 $\times$ l $\times$ C, where $[\theta]_{obs}$ is the ellipticity measured in degrees, mrw is the mean residue molecular weight, C is the protein concentration in g mL^{-1} and l is the optical path length of the cell in cm. A 0.1 cm path length cell was used in the far-UV region. CD spectra were recorded with a time constant of 4 s, a 2 nm band width, and a scan rate of 5 nm min^{-1}, were signal-averaged over at least five scans, and baseline corrected by subtracting a buffer spectrum. The GuHCl-induced denaturation curves at constant temperature were obtained by recording the CD signal at 222 nm for each independent sample. Thermal unfolding curves were recorded in the temperature mode at 222 nm with a scan rate of 1.0 K min^{-1}.

Fluorescence measurements

Steady-state fluorescence measurements were performed with a JASCO FP-750 spectrofluorimeter equipped with thermostated cell holders and temperature was kept constant by a circulating water bath. The excitation wavelength was set at 278 nm in order to include the contribution of Tyr residues to the overall fluorescence emission. The experiments were performed at 25°C by using a 1 cm sealed cell and a 5 nm emission slit width, and corrected for background signal; the shift in fluorescence maximum wavelength was recorded to monitor the unfolding transition.

Sample preparation

The protein solutions were prepared in a 20 mM Tris buffer solution at pH 8.0 and the concentration determined by UV spectra using a theoretical, sequence-based (Gill and von Hippel 1989), extinction coefficient of 29500 M^{-1} cm^{-1} at 278 nm. Stock solutions of GuHCl, in different amounts, were mixed with protein solution to give constant, fixed final protein concentration. Each sample was mixed by vortexing and incubated at 25°C for a day. Longer incubation times produced identical spectroscopic signals.

Results

Structural features of *Sso*Pox

Although the *Sso*Pox 3D structure has been recently reported it was not analyzed from the viewpoint of determinants of thermal stability (Elias et al. 2008). The structure of the monomeric protein, shown in Fig. 1a and b, is roughly globular with overall dimensions of approximately 40 Å $\times$ 54 Å $\times$ 46 Å and its topology is similar to that of the two previously solved structures of mesophilic PTEs: one is from *P. diminuta* and the other is from *A. radiobacter*. The structure could be described as a

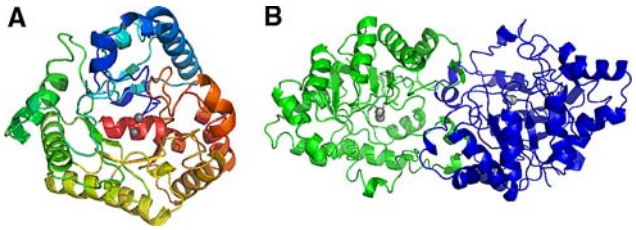

Fig. 1 Structure of *Sso*Pox. **a** The monomer of *Sso*Pox is shown in *cartoon* representation. The two metal cations are shown by *grey spheres*. **b** *Sso*Pox dimer. The two monomers are highlighted in *green* and *blue* and the metal cation active site are shown as *grey balls* (color in online)

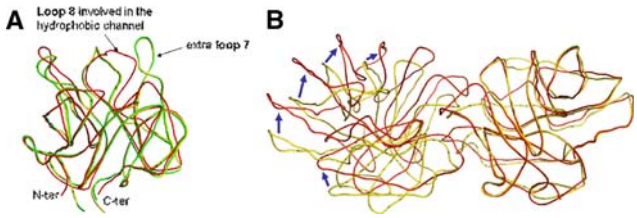

Fig. 2 Structural superposition. **a** Structural comparison of different known PTEs: hyperthermophilic *Sso*Pox in *red*, *P. diminuta* PTE in *yellow* and *A. radiobacter* PTE in *green*. The major structural differences, the absence of the 15 residues loop 7 in *Sso*Pox structure, and the loop 8 involved in the hydrophobic channel are shown by *arrows*. C-terminal and N-terminal extremities of backbones are indicated. **b** Structural comparison between the hyperthermophilic *Sso*Pox (in *red*) and the mesophilic *P. diminuta* PTE (in *yellow*) homodimers. Monomers on the right are well superimposed, whereas there is a shift concerning monomers on the *left*, indicated by *blue arrows* (color in online)

distorted $(\beta/\alpha)_8$ barrel or a so-called TIM barrel (Farber and Petsko 1990). The structure of the hyperthermostable enzyme consists in eight parallel β-strands forming the barrel, flanked on the outer surface by 11 α-helices. The superposition of the solved structures gives r.m.s.d. values for α-carbon atom positions between *Sso*Pox and *P. diminuta* PTE (over 268 atoms), and *Sso*Pox and *A. radiobacter* PTE (over 271 atoms) of 1.05 Å and 1.11 Å, respectively.

Some structural differences are shown in Fig. 2a. There are two shortenings of the *Sso*Pox polypeptide chain compared to the mesophilic PTE structures (note that *Sso*Pox consists of 314 residues, while *P. diminuta* PTE consists of 336 residues). The first one is located close to the entry of the active site and consists in the deletion of a 15-residue loop, which corresponds to loop 7 in the $(\beta/\alpha)_8$ barrel topology. However, thermal stabilization is probably not the major explanation for the shortening of this loop because it has been shown to be crucial in the differentiation between lactonase and PTE specificities (Elias et al. 2008). The second one is the shortening of both extremities of the polypeptide chain. In fact, compared to mesophilic PTEs, *Sso*Pox has 6 and 2 residues less at the C terminus extremity, and 2 and 4 residues less at the N terminus extremity with respect to *P. diminuta* PTE and *A. radiobacter* PTE, respectively.

As observed for both mesophilic PTEs, *Sso*Pox crystallizes as a homo-dimer whose structural organization is shown in Fig. 2b. In particular, the loop from Tyr97 to Ser110 in each monomer adopts a different conformation with respect to the corresponding loop from Trp131 to Ser142 of *P. diminuta* PTE, markedly protruding in and interacting with the other subunit. Thus, across the interface, there are two large hydrophobic clusters, each constituted by the side chains of Phe104 and Leu107 of one subunit, and Tyr97, Tyr99 and Trp263 of the other subunit, tightly anchoring the two monomers to each other in the *Sso*Pox structure.

For the two mesophilic PTEs, the contact area between the monomers is around 1350 $Å^2$, 62.5% of which consists of hydrophobic contacts, and there are 25 hydrogen bonds across the interface. In the *Sso*Pox structure the interactions cited lead to an interpenetration of the two monomers and a consequent increase in contact area. The latter amounts to 1720 $Å^2$ and the extra contact area, i.e. 370 $Å^2$, is mainly due to additional hydrophobic contacts. In fact, the number of hydrogen bonds across the interface is 25, the same number observed in mesophilic PTEs. The solvent accessibility of *Sso*Pox is reduced with respect to that of its mesophilic counterparts because the quaternary organization of the *Sso*Pox dimer is different from that of the two mesophilic PTEs. As emphasized in Fig. 2b, on superimposing the monomers on the right, the other subunit of *Sso*Pox is significantly rotated with respect to that of *P. diminuta* PTE.

Electrostatic features of *Sso*Pox

Analysis of *Sso*Pox sequence reveals that there is a decrease in the content of uncharged polar residues Gln, Asn, Thr and Ser with respect to mesophilic counterparts. These residues represent 15.9% of the total residues of the hyperthermostable sequence, compared to 18.3 and 19.7% in the *P. diminuta* and *A. radiobacter* PTE sequences, respectively. This difference is expected on comparing hyperthermophilic and mesophilic proteins. Gln and Asn residues, in fact, are prone to deamidation, that can be catalyzed by close Ser and Thr residues, and to cleavage of the peptide bond, especially at temperatures approaching or above 90°C (Wright 1991). It is plausible that these weak points are protected or replaced particularly in hyperthermophilic proteins. Accordingly there is an overall reduction in the content of Asn and Gln residues in the majority of hyperthermophilic proteins (Szilagyi and Zavodszky 2000).

In addition, *Sso*Pox sequence shows an increase in the content of charged residues: Asp, Glu, Lys and Arg

represent 24.5% of the total residues in *Sso*Pox sequence, whereas this value is about 21% for both mesophilic PTEs. The 3D structure shows that the extra charges are mainly located in solvent-accessible regions of *Sso*Pox surface.

Therefore, *Sso*Pox is a highly charged protein: 39 (Asp + Glu) and 37 (Lys + Arg) residues are localized on the protein surface. Half of these surface charged residues are involved in salt bridges: *Sso*Pox contains 25 salt bridges per monomer compared to 15 salt bridges per monomer for both mesophilic PTEs (using a cut-off distance of 4 Å). By looking at the electrostatic potential (see "Materials and methods") one face of the protein is essentially negatively charged, and the other possesses large positively charged clusters. This charge repartition may confer to the protein a very high dipolar moment (Fig. 3a). Furthermore, the border area between the two monomers is almost homogeneously negatively charged. This fact is surprising, because non-complementary charge interactions should increase the repulsion energy. However, they might be stabilizing in the electrostatic field created by the charge configuration in the protein, especially considering charges in a dynamic context at high temperature (Danciulescu et al. 2007).

Only one region of the protein is little electrostatically charged. This is a hydrophobic pocket, corresponding to the active site, and surrounded by negative charges.

The salt bridges are uniformly localized on the protein surface (see Fig. 3b) and, as described for other hyperthermophilic proteins (Hennig et al. 1997; Goldman 1995), most of them are involved in large and complex networks of charge–charge interactions. Two such networks, that involving Asp43-Lys81-Asp42-Arg26-Asp75-Arg33-Glu45 and that involving Glu150-Arg154-Glu188-Lys161-Glu187-Arg183-Glu180 are shown in Fig. 3c. In addition, in each monomer of *Sso*Pox, (a) the two chain termini are linked by a salt bridge (the distance between the charges is 3.9 Å) between the terminal carboxylic group of Ser314 and the guanidinium group of Arg2; (b) the presence of Pro residues at position 4 and 309 further confers rigidity to the chain termini. This kind of mutual stabilization for N and C termini, also seen in *Thermotoga maritima* phosphoribosyl anthranilate isomerase (Hennig et al. 1997), is assumed to increase the protein overall stability since chain termini can be the starting point of unfolding. There are also two salt bridges, on opposite parts of the interface, between the carboxylic group of Glu113 of one monomer with the side

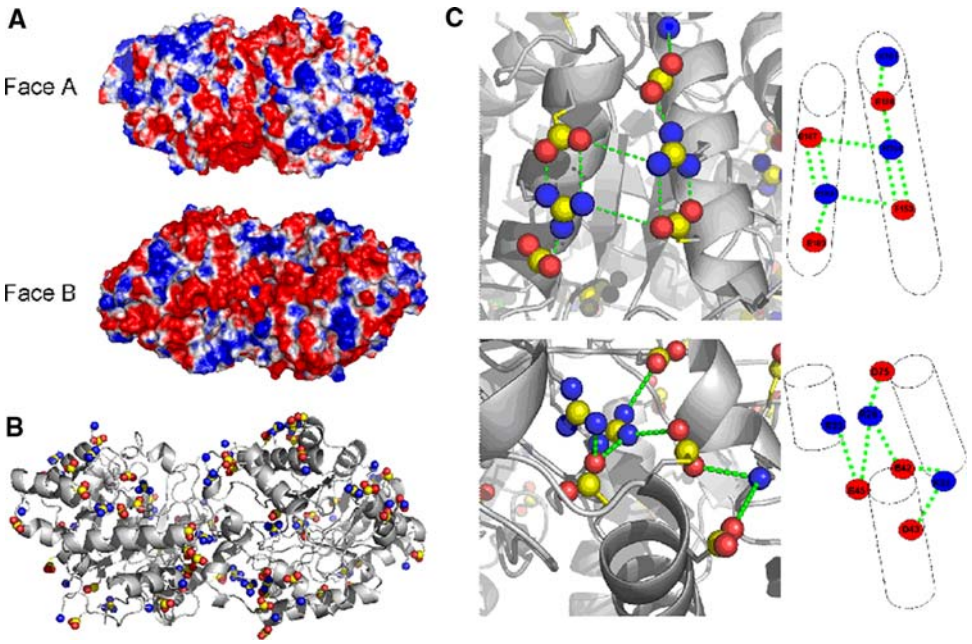

Fig. 3 Electrostatic charges and active site description. **a** Electrostatic potential computed using MoPro is shown at the molecular surface of *Sso*Pox homodimer. Both faces of the homodimer are shown. Negatively charged areas are in *red*, positively charged areas in *blue*, non-charged areas in *white*. **b** Ribbon representation of *Sso*Pox homodimer. The main chain is in *grey*. All charged chemical functions in electrostatic interaction are highlighted (distance cut-off between charged atoms: 5 Å). Positively charged residues (Arg and Lys) and negatively charged ones (Asp, Glu and terminal carboxylic acid) are shown as *spheres*. Carbon atoms are in *yellow*, oxygen atoms in *red*, nitrogen atoms in *blue*. Most of the salt bridges are on the protein surface. **c** Ribbon representation of two charge–charge networks. *On the left* the main chain is colored in *grey*. Interactions between complementary charges are indicated by *green dash*. As in **b**, positively charged residues (Arg and Lys) and negatively ones (Asp, Glu and terminal carboxylic acid) are shown in as *spheres*. Carbon atoms are in *yellow*, oxygen atoms in *red*, nitrogen atoms in *blue*. *On the right* a simplified scheme of a charge–charge network. α-helices are shown as *rolls*, charged groups as *ovals*. Positively charged groups are in *blue*, negatively charged in *red*. Number and type of residues involved are indicated (color in online)

chain NH2 group of Lys267 of the other monomer, that protect the interface from water penetration.

Conformational stability of *Sso*Pox

*Sso*Pox is a highly thermostable enzyme, as it is active toward paraoxon up to high temperature (Merone et al. 2005). A maximum for activity could not be determined because of technical limitations, but up to 95°C, the activity still keeps increasing. This datum should be supported by a more detailed investigation of the conformational stability of *Sso*Pox by means of circular dichroism (CD) and fluorescence measurements (Del Vecchio et al. 2002a, b, 2004).

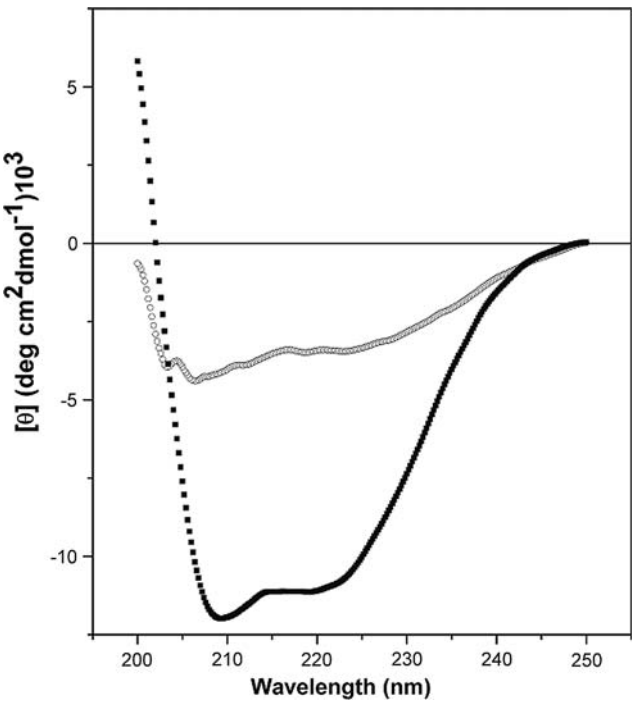

Fig. 4 Far-UV CD spectra of *Sso*Pox. Spectra were acquired at 25°C (*filled squares*) and 108°C (*open circles*) with a protein concentration of 0.13 mg mL^{-1}

The far-UV CD spectra of *Sso*Pox at 25 and 108°C, pH 8.0, are shown in Fig. 4. The spectrum of native *Sso*Pox presents a double minimum at 208 and 222 nm, as expected for a protein with the large α-helical content characteristic of a distorted $(\beta/\alpha)_8$ barrel. The spectrum of *Sso*Pox at 108°C is completely different, indicating a marked loss of secondary structure elements, even though it does not correspond to that of a random coil. It is worth noting that these far-UV CD spectra correspond to those reported for *P. diminuta* PTE by Grimsley et al. (1997).

By recording the molar ellipticity at 222 nm it has not been possible to obtain complete thermal denaturation curves because the transition is not yet finished at 108°C (see curve a in Fig. 5a), and our instrumental set-up cannot work at temperatures higher than 110°C. This datum confirms the very high thermal stability of *Sso*Pox inferred from enzymatic activity measurements. In order to obtain complete thermal denaturation curves, *Sso*Pox has been incubated with different GuHCl concentrations to somewhat destabilize the native state. The corresponding thermal denaturation curves are shown in Fig. 5a and the denaturation temperatures are (using a constant protein concentration of 0.2 mg mL^{-1}): 97°C at 0.5 M GuHCl, 92°C at 0.8 M GuHCl, 89°C at 1 M GuHCl, 80°C at 1.5 M GuHCl, 73°C at 2 M GuHCl, and 62°C at 2.5 M GuHCl. By performing a linear extrapolation of these numbers up to zero GuHCl concentration, the estimated denaturation temperature of *Sso*Pox is 106°C (see Fig. 5b).

It has to be noted that thermal denaturation of *Sso*Pox is not reversible in all the investigated experimental conditions, and so no further thermodynamic analysis of thermal denaturation curves has been done. In any case, since the

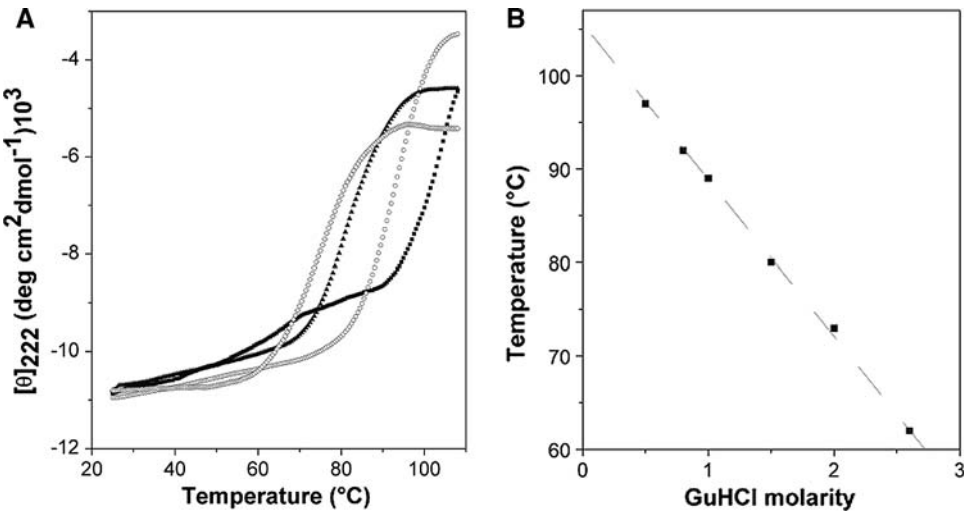

Fig. 5 Thermal denaturation of *Sso*Pox by CD analysis. **a** Thermal denaturation curves of *Sso*Pox (constant protein concentration of 0.2 mg mL^{-1}), by recording the molar ellipticity at 222 nm with zero GuHCl (*filled squares*), 0.8 M GuHCl (*open circles*), 1.5 M GuHCl (*filled triangles*), and 2 M GuHCl (*open diamonds*). **b** Plot of *Sso*Pox denaturation temperatures versus the GuHCl concentration to obtain by extrapolation an estimate of the stability in aqueous solution

denaturation temperature of *P. diminuta* PTE is 75°C, these results highlight the significant extra thermal stability of *Sso*Pox.

The conformational stability of *Sso*Pox against the denaturing action of GuHCl has been investigated at 25°C, pH 8.0, 20 mM Tris–HCl buffer, by performing CD and fluorescence measurements (note that urea cannot be used because the enzyme proves to be extremely resistant to this chemical denaturant). The transition curves obtained by recording the molar ellipticity at 222 nm (i.e., detecting the secondary structure stability) present two inflection points, at 2.6 M GuHCl and about 4.8 M GuHCl, respectively, with a plateau at about 3 M GuHCl (see Fig. 6a). Since *Sso*Pox is a homodimer in which the association of the two subunits is provided by noncovalent interactions, the unfolded state has to correspond to two unfolded monomers. In addition, the two inflection points and the plateau region are suggestive of the presence of an intermediate along the unfolding-denaturation pathway of *Sso*Pox. Therefore, a dependence on protein concentration of the location of one or both of the inflection points has to be expected. Measurements have demonstrated that the location of the first inflection point does not depend on protein concentration, while the location of the second inflection point does (see Fig. 6a). This means that the intermediate is a dimeric species and that dissociation occurs in the second step of the process. The comparison between *Sso*Pox and *P. diminuta* PTE shows that the two inflection points occur at the markedly higher GuHCl concentration in the case of the hyperthermophilic enzyme. At a protein concentration of 0.13 mg mL^{-1} the inflection points are: 1 versus 2.6 M GuHCl, and 2.5 versus 5 M GuHCl, respectively. These data clarify that *Sso*Pox is markedly more resistant to the denaturing action of GuHCl with respect to the mesophilic counterpart; in particular, the dimeric intermediate of *Sso*Pox does appear to be much more stable than that of *P. diminuta* PTE.

In order to probe the stability of the tertiary structure, GuHCl-induced transition curves have been determined by recording the shift in the wavelength corresponding to the maximum of the fluorescence emission spectrum, λ_{max}, upon excitation at 278 nm. Since each monomer of *Sso*Pox contains 3 Trp residues (at position 36, 263 and 278) and 9 Tyr residues (at position 40, 97, 99, 105, 208, 224, 247, 257 and 270), it was decided to fix the excitation wavelength at 278 nm in order to detect the contribution of both the 9 Tyr and 3 Trp residues to the fluorescence emission. Also the transition curves reporting λ_{max} versus GuHCl concentration, at 25°C, pH 8.0, 20 mM Tris-HCl buffer, present two inflection points, as those constructed by recording the molar ellipticity at 222 nm. The location of the first inflection point does not depend on protein concentration and occurs always at 2.6 M GuHCl, while that of the second inflection point depends on protein concentration and occurs always above 4.5 M GuHCl (see Fig. 6b). All these findings are in agreement with the unfolding-denaturation pathway proposed on the basis of far-UV CD data, suggesting the presence of a dimeric intermediate stable at about 3 M GuHCl.

It is worth noting that λ_{max} upon excitation at 278 nm amounts to 335 nm for native *Sso*Pox, 343 nm for the dimeric intermediate, and 352 nm for the unfolded

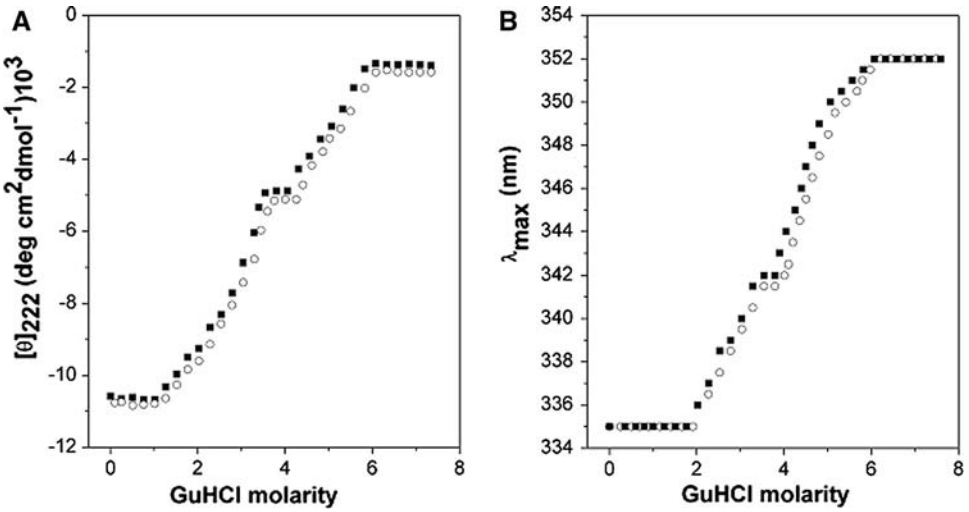

Fig. 6 GuHCl-induced denaturation of *Sso*Pox by CD analysis. **a** GuHCl-induced denaturation curves of *Sso*Pox, constructed by recording the molar ellipticity at 222 nm and 25°C, at two protein concentrations, 0.7 mg mL^{-1} (*filled squares*) and 1.3 mg mL^{-1} (*open circles*). **b** GuHCl-induced denaturation curves of *Sso*Pox, constructed by recording the shift in the wavelength of the maximum of fluorescence spectrum upon excitation at 278 nm and 25°C, at two protein concentrations, 0.6 mg mL^{-1} (*filled squares*) and 1.0 (*open circles*) mg mL^{-1}

monomeric species. The λ_{max} value of native *Sso*Pox indicates that the 3 Trp residues present in each monomer are buried in the protein interior, whereas the other two λ_{max} values are indicative of a partial exposure to water contact in the dimeric intermediate, and a complete exposure in the unfolded monomeric species (Lakowicz 1983).

The overall GuHCl-induced denaturation of *Sso*Pox is not a reversible process in all the investigated experimental conditions: upon suitable dilution of fully denatured samples, there is not a complete recovery of the far-UV CD spectrum or fluorescence emission spectrum of the native enzyme. This irreversibility impairs a correct thermodynamic analysis of the GuHCl-induced transition curves of *Sso*Pox according, for instance, to the linear extrapolation model. In any case, the location of the two inflection points, being the direct experimental datum, should be considered a correct quantitative measure of the protein stability against the denaturing action of GuHCl.

Discussion

*Sso*Pox is a hyperthermostable protein: its activity is still increasing at 95°C, in line with the estimated denaturation temperature of 106°C, and the strong resistance to the denaturing action of urea. The GuHCl-induced denaturation curves of *Sso*Pox present two inflection points and can be rationalized by the presence of a dimeric intermediate that eventually dissociates leading to two unfolded monomers. The unfolding-denaturation pathway of *Sso*Pox can be described by the following scheme:

$$N_2 \Rightarrow I_2 \Rightarrow 2U$$

It is worth noting that this is the same unfolding-denaturation pathway determined for *P. diminuta* PTE by Grimsley et al. (1997) but the GuHCl concentrations corresponding to the two inflection points are much more high in the case of *Sso*Pox.

The structural comparison between the 3D structure of *Sso*Pox and the structures of its mesophilic homologues from *A. radiobacter* and *P. diminuta* has revealed interesting features concerning the structural adaptation of this architecture to extreme conditions. The fundamental differences are: (a) *Sso*Pox possesses a tighter and more compact quaternary structure due to an optimization of the interactions at the interface between the two monomers; (b) *Sso*Pox possesses a larger number of surface salt bridges, also involved in complex networks.

The distinct conformation adopted by the loop starting with Tyr97 and ending at Ser110 in each monomer of *Sso*Pox allows an optimization of interface interactions between the subunits, and should be very important for the conformational stability of the dimeric structure. Indeed CD and fluorescence measurements indicate that *Sso*Pox is much more stable than the mesophilic *P. diminuta* PTE with respect to both temperature and GuHCl. In particular, the dimeric intermediate populated along the unfolding-denaturation pathway of *Sso*Pox is stable around 3 M GuHCl, a denaturant concentration at which *P. diminuta* PTE is completely unfolded. This should be a strong indication of the stabilization provided by the tightening of the interactions across the interface. Such conclusion is supported by the finding that the two mesophilic and the hyperthermophilic monomers are similar in size, but the thermostable dimer is more compact than the two mesophilic dimers (i.e., the volume of *Sso*Pox is reduced with respect to mesophilic homologues, as emphasized in Fig. 3b). Minimization of the ratio of surface area to volume can increase the stability by simultaneously reducing the unfavorable surface energy and increasing the attractive interior packing interactions (Chan et al. 1995). Reinforcement of interactions at the interface supports the contention that dimerization could be a general determinant of thermostabilization (Vieille and Zeikus 2001). More specifically high oligomeric state is a striking preference for thermoadaptation of hyperthermophiles, as it was seen for TIM protein (Walden et al. 2004).

In addition, the interface hydrophobicity can be important since hydrophobic interactions are strengthened at high temperatures (Lo Conte et al. 1999), so that the homodimeric structure of *Sso*Pox should be functionally relevant in the archaeal cell.

The other fundamental difference between *Sso*Pox and its mesophilic counterparts is the larger number of salt bridges, 25 versus 15 in each monomer, and their organization in complex networks on the protein surface. This finding is in line with general analyses that have compared the structures of hyperthermophilic, thermophilic and mesophilic proteins (Vetriani et al. 1998; Karshikoff and Ladenstein 2001; Sterner and Liebl 2001; De Simone et al. 2001).

These observations correlate with previous general findings: (a) the surfaces of hyperthermophilic proteins show an increase in charged residues at the expense of polar residues (Szilagyi and Zavodszky 2000); (b) the comparison of complete genomes of mesophiles and hyperthermophiles indicates a large difference in the proportions of charged residues versus uncharged polar residues (Fukuchi and Nishikawa 2001; Suhre and Claverie 2003).

In addition, the stabilizing role of the large and complex charge–charge networks in *Sso*Pox is supported by the fact that it is extremely resistant to the action of a neutral denaturant such as urea, whereas it is unfolded by a ionic denaturant such as GuHCl (Del Vecchio et al. 2002a, b). The presence of large and complex charge–charge

networks suggests that cooperative-multiple electrostatic interactions are more efficient to enhance thermostability than a sum of pair-wise interactions. It is important to note that all the archaeal TIM barrel proteins previously described do not exploit an increase of salt bridges for achieving thermoadaptation (Walden et al. 2004). Therefore, the hyperthermophilic *Sso*Pox is, to the best of our knowledge, the first archaeal hyperthermophilic TIM barrel protein that has a significantly larger number of salt bridges and complex charge–charge networks with respect to its mesophilic counterparts.

Owing to its thermostability and unique catalytic properties, *Sso*Pox is an excellent candidate to construct an efficient biodecontaminant of organophosphorous compounds and also a potential weapon against pathogens that use "quorum sensing" as an infectiveness tool (Dong et al. 2001). The present study could be an important step to try to adapt the catalytic properties of *Sso*Pox to industrial uses.

Acknowledgments This research was supported by grants to E.C. by Délégation Générale pour l'Armement (CO no. 010807/03-10) and by the C.N.R.S. D.R. is under contract with Bundesministerium der Verteidigung (M/SAB/1/7/A004). We also thank MIUR project "Piano Nazionale Ricerca per le Biotecnologie Avanzate Tema II, Biocatalisi".

References

Afriat L, Roodveldt C, Manco G, Tawfik DS (2006) The latent promiscuity of newly identified microbial lactonases is linked to a recently diverged phosphotriesterase. Biochemistry 45:13677–13686

Aubert SD, Li Y, Raushel FM (2004) Mechanism for the hydrolysis of organophosphates by the bacterial phosphotriesterase. Biochemistry 43:5707–5715

Bruins ME, Janssen AE, Boom RM (2001) Thermozymes and their applications: a review of recent literature and patents. Appl Biochem Biotechnol 90:155–186

Chan MK, Mukund S, Kletzin A, Adams MW, Rees DC (1995) Structure of a hyperthermophilic tungstopterin enzyme, aldehyde ferredoxin oxidoreductase. Science 267:1463–1469

Cheng TC, Harvey SP, Stroup AN (1993) Purification and properties of a highly active organophosphorus acid anhydrolase from *Alteromonas undina*. Appl Environ Microbiol 59:3138–3140

D'Amico S, Marx JC, Gerday C, Feller G (2003) Activity–stability relationships in extremophilic enzymes. J Biol Chem 278:7891–7896

Danciulescu C, Ladenstein R, Nilsson L (2007) Dynamic arrangement of ion pairs and individual contributions to the thermal stability of the cofactor-binding domain of glutamate dehydrogenase from *Thermotoga maritima*. Biochemistry 46:8537–8549

De Simone G, Menchise V, Manco G, Mandrich L, Sorrentino N, Lang D, Rossi M, Pedone C (2001) The crystal structure of a hyper-thermophilic carboxylesterase from the archaeon *Archaeoglobus fulgidus*. J Mol Biol 314:507–518

Del Vecchio P, Graziano G, Granata V, Barone G, Mandrich L, Manco G, Rossi M (2002a) Temperature- and denaturant-induced unfolding of two thermophilic esterases. Biochemistry 41:1364–1371

Del Vecchio P, Graziano G, Granata V, Barone G, Mandrich L, Rossi M, Manco G (2002b) Denaturing action of urea and guanidine hydrochloride towards two thermophilic esterases. Biochem J 367:857–863

Del Vecchio P, Graziano G, Granata V, Farias T, Barone G, Mandrich L, Rossi M, Manco G (2004) Denaturant-induced unfolding of the acetyl-esterase from *Escherichia coli*. Biochemistry 43:14637–14643

DeLano WL (2002) The PyMOL molecular graphics system DeLano scientific. San Carlos, CA

Demirjian DC, Moris-Varas F, Cassidy CS (2001) Enzymes from extremophiles. Curr Opin Chem Biol 5:144–151

Dong Y-H, Wang L-H, Xu J-L, Zhang H-B, Zhang X-F, Zhang L-H (2001) Quenching quorum-sensing-dependent bacterial infection by an *N*-acyl homoserine lactonase. Nature 411:813–817

Elias M, Dupuy J, Merone L, Lecomte C, Rossi M, Masson P, Manco G, Chabriere E (2007) Crystallization and preliminary X-ray diffraction analysis of the hyperthermophilic *Sulfolobus solfataricus* phosphotriesterase. Acta Crystallograph Sect F Struct Biol Cryst Commun 63:553–555

Elias M, Dupuy J, Merone L, Mandrich L, Porzio E, Moniot S, Rochu D, Lecomte C, Rossi M, Masson P, Manco G, Chabriere E (2008) Structural basis for natural lactonase and promiscuous phosphotriesterase activities. J Mol Biol 379:1017–1028

Farber GK, Petsko GA (1990) The evolution of alpha/beta barrel enzymes. Trends Biochem Sci 15:228–234

Fukuchi S, Nishikawa K (2001) Protein surface amino acid compositions distinctively differ between thermophilic and mesophilic bacteria. J Mol Biol 309:835–843

Ghanem E, Raushel FM (2005) Detoxification of organophosphate nerve agents by bacterial phosphotriesterase. Toxicol Appl Pharmacol 207:459–470

Gill SC, von Hippel PH (1989) Calculation of protein extinction coefficients from amino acid sequence data. Anal Biochem 182:319–326

Goldman A (1995) How to make my blood boil. Structure 3:1277–1279

Grimsley JK, Scholtz JM, Pace CN, Wild JR (1997) Organophosphorus hydrolase is a remarkably stable enzyme that unfolds through a homodimeric intermediate. Biochemistry 36:14366–14374

Guex N, Peitsch MC (1997) SWISS-MODEL and the Swiss-PdbViewer: an environment for comparative protein modeling. Electrophoresis 18:2714–2723

Guillot B, Lecomte C, Cousson A, Scherf C, Jelsch C (2001) High-resolution neutron structure of nicotinamide adenine dinucleotide. Acta Crystallogr D Biol Crystallogr 57:981–989

Harel M, Aharoni A, Gaidukov L, Brumshtein B, Khersonsky O, Meged R, Dvir H, Ravelli RB, McCarthy A, Toker L, Silman I, Sussman JL, Tawfik DS (2004) Structure and evolution of the serum paraoxonase family of detoxifying and anti-atherosclerotic enzymes. Nat Struct Mol Biol 11:412–419

Hennig M, Sterner R, Kirschner K, Jansonius JN (1997) Crystal structure at 2.0 Å resolution of phosphoribosyl anthranilate isomerase from the hyperthermophile *Thermotoga maritima*: possible determinants of protein stability. Biochemistry 36:6009–6016

Horne I, Qiu X, Russell RJ, Oakeshott JG (2003) The phosphotriesterase gene opdA in *Agrobacterium radiobacter* P230 is transposable. FEMS Microbiol Lett 222:1–8

Hou X, Maser RL, Magenheimer BS, Calvet JP (1996) A mouse kidney- and liver-expressed cDNA having homology with a prokaryotic parathion hydrolase (phosphotriesterase)-encoding gene: abnormal expression in injured and polycystic kidneys. Gene 168:157–163

Jackson C, Kim HK, Carr PD, Liu JW, Ollis DL (2005) The structure of an enzyme-product complex reveals the critical role of a

terminal hydroxide nucleophile in the bacterial phosphotriesterase mechanism. Biochim Biophys Acta 1752:56–64
Jackson CJ, Foo JL, Kim HK, Carr PD, Liu JW, Salem G, Ollis DL (2008) In crystallo capture of a Michaelis complex and product-binding modes of a bacterial phosphotriesterase. J Mol Biol 375:1189–1196
Jaenicke R, Bohm G (1998) The stability of proteins in extreme environments. Curr Opin Struct Biol 8:738–748
Jones S, Thornton JM (1996) Principles of protein–protein interactions. Proc Natl Acad Sci USA 93:13–20
Karshikoff A, Ladenstein R (2001) Ion pairs and the thermotolerance of proteins from hyperthermophiles: a "traffic rule" for hot roads. Trends Biochem Sci 26:550–556
Koepke J, Scharff EI, Lucke C, Ruterjans H, Fritzsch G (2002) Atomic resolution crystal structure of squid ganglion DFPase. Acta Crystallogr D Biol Crystallogr 58:1757–1759
Ladenstein R, Antranikian G (1998) Proteins from hyperthermophiles: stability and enzymatic catalysis close to the boiling point of water. Adv Biochem Eng Biotechnol 61:37–85
Lakowicz JR (1983) Principles of fluorescence spectroscopy. Plenum Press, New York
LeJeune KE, Wild JR, Russell AJ (1998) Nerve agents degraded by enzymatic foams. Nature 395:27–28
Lo Conte L, Chothia C, Janin J (1999) The atomic structure of protein–protein recognition sites. J Mol Biol 285:2177–2198
McDonald IK, Thornton JM (1994) Satisfying hydrogen bonding potential in proteins. J Mol Biol 238:777–793
Merone L, Mandrich L, Rossi M, Manco G (2005) A thermostable phosphotriesterase from the archaeon *Sulfolobus solfataricus*: cloning, overexpression and properties. Extremophiles 9:297–305
Merone L, Mandrich L, Rossi M, Manco G (2008) Enzymes with phosphotriesterase and lactonase activities in Archaea. Current Chem Biol 2:237–248
Munnecke DM (1976) Enzymatic hydrolysis of organophosphate insecticides, a possible pesticide disposal method. Appl Environ Microbiol 32:7–13
Murshudov N, Vagin AA, Dodson EJ (1997) Refinement of macromolecular structures by the maximum-likelihood method. Acta Crystallogr D Biol Crystallogr 53:240–255
Pichon-Pesme V, Jelsch C, Guillot B, Lecomte C (2004) A comparison between experimental and theoretical aspherical-atom scattering factors for charge–density refinement of large molecules. Acta Crystallogr A 60:204–208
Raushel FM (2002) Bacterial detoxification of organophosphate nerve agents. Curr Opin Microbiol 5:288–295
Rothschild LJ, Mancinelli RL (2001) Life in extreme environments. Nature 409:1092–1101
Seibert CM, Raushel FM (2005) Structural and catalytic diversity within the amidohydrolase superfamily. Biochemistry 44:6383–6391
Sethunathan N, Yoshida T (1973) A Flavobacterium sp. that degrades diazinon and parathion. Can J Microbiol 19:873–875
Singh BK (2009) Organophosphorus-degrading bacteria: ecology and industrial applications. Nat Rev Microbiol 7:156–164
Sterner R, Liebl W (2001) Thermophilic adaptation of proteins. Crit Rev Biochem Mol Biol 36:39–106
Suhre K, Claverie JM (2003) Genomic correlates of hyperthermostability, an update. J Biol Chem 278:17198–17202
Szilagyi A, Zavodszky P (2000) Structural differences between mesophilic, moderately thermophilic and extremely thermophilic protein subunits: results of a comprehensive survey. Structure 8:493–504
Vetriani C, Maeder DL, Tolliday N, Yip KS, Stillman TJ, Britton KL, Rice DW, Klump HH, Robb FT (1998) Protein thermostability above 100 degrees C: a key role for ionic interactions. Proc Natl Acad Sci USA 95:12300–12305
Vieille C, Zeikus GJ (2001) Hyperthermophilic enzymes: sources, uses, and molecular mechanisms for thermostability. Microbiol Mol Biol Rev 65:1–43
Walden H, Taylor GL, Lorentzen E, Pohl E, Lilie H, Schramm A, Knura T, Stubbe K, Tjaden B, Hensel R (2004) Structure and function of a regulated archaeal triosephosphate isomerase adapted to high temperature. J Mol Biol 342:861–875
Willard L, Ranjan A, Zhang H, Monzavi H, Boyko RF, Sykes BD, Wishart DS (2003) VADAR: a web server for quantitative evaluation of protein structure quality. Nucleic Acids Res 31:3316–3319
Wong KY, Gao J (2007) The reaction mechanism of paraoxon hydrolysis by phosphotriesterase from combined QM/MM simulations. Biochemistry 46:13352–13369
Wright HT (1991) Sequence and structure determinants of the nonenzymatic deamidation of asparagine and glutamine residues in proteins. Protein Eng 4:283–294